Journal of Materials Chemistry

Cite this: *J. Mater. Chem.*, 2011, **21**, 15843

www.rsc.org/materials

HIGHLIGHT

Phonon engineering through crystal chemistry†

Eric S. Toberer,* Alex Zevalkink and G. Jeffrey Snyder*

DOI: 10.1039/c1jm11754h

Mitigation of the global energy crisis requires tailoring the thermal conductivity of materials. Low thermal conductivity is critical in a broad range of energy conversion technologies, including thermoelectrics and thermal barrier coatings. Here, we review the chemical trends and explore the origins of low thermal conductivity in crystalline materials. A unifying feature in the latest materials is the incorporation of structural complexity to decrease the phonon velocity and increase scattering. With this understanding, strategies for combining these mechanisms can be formulated for designing new materials with exceptionally low thermal conductivity.

Introduction

Controlling heat flow is critical to applications ranging from jet turbines to microelectronics to thermoelectrics. In energy applications, thermal engineering frequently determines system efficiency, lifetime, and cost. For example, thermal barrier coatings enable higher turbine operating temperature, thereby increasing the Carnot efficiency.[1–3] In thermoelectrics, dramatic improvements in efficiency have been driven by reductions in thermal conductivity.[4–8] The discovery of complex, bulk thermoelectric materials with low thermal conductivity (*e.g.*, $Yb_{14}MnSb_{11}$, $Ba_8Ga_{16}Ge_{30}$, $X_yCo_4Sb_{12}$) has led to a renewed investigation of the fundamental mechanisms of thermal conductivity.[14–17] Similar low thermal conductivity has been found in thermal barrier coating materials ($La_2Mo_2O_9$, $W_3Nb_{14}O_{44}$).[18]

Understanding the origins of this behavior is important for the development of advanced materials. The complexity of these materials, however, makes *ab initio* calculations of lattice dynamics prohibitively difficult.[19–24] Here we use simple models for heat transport to approximate the complex interplay of phonon scattering and group velocity. Despite these approximations, these models highlight the critical *material parameters* that ultimately determine thermal conductivity.

Thermal conductivity in a material arises from both electronic (κ_e) and lattice (κ_L) contributions.[25–28] The electronic component is well described by the Wiedemann–Franz law, scaling linearly with the electrical conductivity and temperature. The lattice contribution arises from lattice vibrations (phonons) and is the subject of this review.

To lay the groundwork for a more in-depth examination of factors affecting lattice thermal conductivity, we consider eqn (1), which describes κ_L as the product of heat capacity (C_v), phonon velocity (v), and phonon mean free path (l). This equation provides a rough guide to κ_L, despite neglecting the frequency dependence of each parameter. The phonon relaxation time, τ, is related to l through the phonon velocity. The phonon velocity is often simply approximated by the low frequency speed of sound ($v_s \propto \sqrt{B/\delta}$), where B is the appropriate elastic modulus and δ is the density of the material.

$$\kappa_L = \frac{1}{3} C_v v l = \frac{1}{3} C_v v^2 \tau \qquad (v = l/\tau) \quad (1)$$

Traditionally, achieving low lattice thermal conductivity has relied on (a) low v_s, found in dense materials with soft bonds, or (b) reduction of τ by the intentional introduction of point defects and nanostructures to scatter phonons.[1,9,10,29–32] Fig. 1 shows the success of these approaches in thermoelectric materials.

While eqn (1) qualitatively describes κ_L, the universal relaxation time and constant velocity used in this model leads to significant inconsistencies and departure from experimental results. Crucial to the development of materials with controlled phonon transport is a frequency-dependent description of κ_L, as all of the terms in eqn (1) vary significantly across the phonon spectrum. Use of a simplified version of the Callaway model gives eqn (2),[33,34] which neglects the small correction term for non-resistive (normal) phonon–phonon interactions.[19,20,26,35]

$$\kappa_L = \frac{1}{3}\int_0^{\omega_{max}} C_s(\omega) v_g(\omega)^2 \tau(\omega) d\omega \qquad (2)$$

The need for frequency-dependent analysis is revealed by considering bulk silicon. Eqn (1) yields $l = 45$ nm at 300 K, using experimental κ_L, heat capacity, and speed of sound. In contrast, eqn (2) indicates that 80% of the lattice thermal conductivity arises from phonons with mean free paths between 0.1–10 μm.[36] This latter result is consistent with

Materials Science, California Institute of Technology, 1200 E, California Blvd. Pasadena, CA, 91125, USA. E-mail: etoberer@mines.edu; jsnyder@caltech.edu

† Electronic supplementary information (ESI) available: Supplementary Table 1. See DOI: 10.1039/c1jm11754h

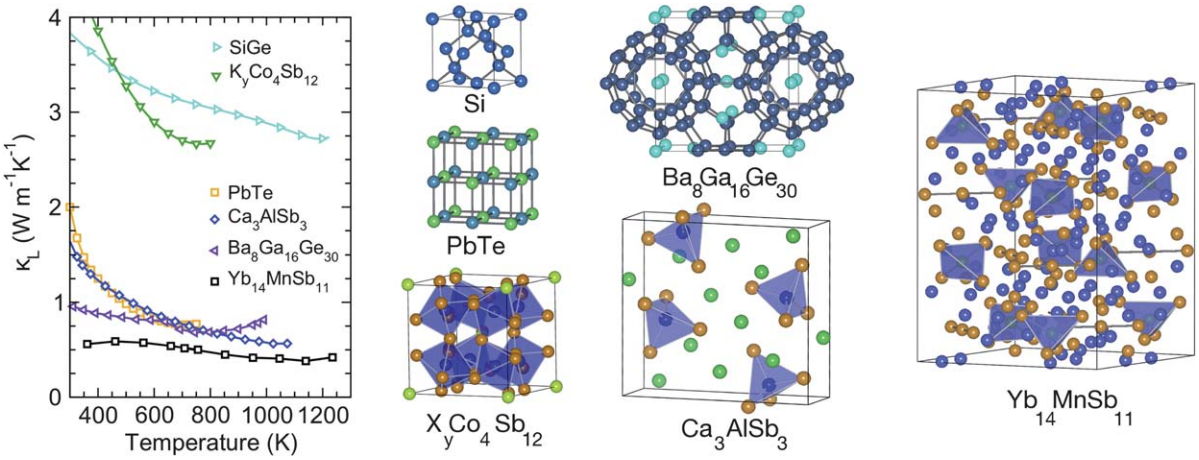

Fig. 1 Thermoelectric materials can achieve low lattice thermal conductivity through point scattering sources ($Si_{1-x}Ge_x$, $X_yCo_4Sb_{12}$), heavy atoms and anharmonic bonding (PbTe) and complex crystal structures, in which most of the phonon dispersion consists of low velocity optical modes ($Yb_{14}MnSb_{11}$, Ca_3AlSb_3, $Ba_8Ga_{16}Ge_{30}$).[9–14]

experimental results which show significant reduction in κ_L when phonon scattering sources are induced at micron length scales.[37]

Here we review the frequency dependence of scattering and highlight the importance of the phonon dispersion in determining κ_L. We begin with a discussion of the *prediction* of lattice thermal conductivity in simple materials where the phonon group velocity can be approximated as constant (Debye model). We then use this understanding to tackle more complex materials where the group velocity is highly frequency-dependent. These examples guide the design and discovery of low thermal conductivity materials.

Thermal conductivity within the Debye model

The Debye model is a reasonable starting point for discussing thermal transport in simple crystalline materials, as it allows us to approximate the phonon group velocity ($v_g = d\omega/dk$) and phase velocity ($v_p = \omega/k$) as the speed of sound, v_s (Fig. 2).[38,39] Here, v_s is the appropriate average of the longitudinal and transverse velocities at the low frequency limit. The Debye model has a maximum phonon frequency given by $\omega_{max} = \omega_D = \left(\frac{6\pi^2}{V}\right)^{1/3} v_s$, where V is the atomic volume. The corresponding Debye temperature is given by $k_B\theta_D = \hbar\omega_D$.

The Debye specific heat capacity is given by eqn (3). We are interested in the *spectral* heat capacity ($C_s(\omega)$), related to the phonon density of states, shown in Fig. 3(a) at various temperatures. At high temperature, the frequency dependence of $C_s(\omega)$ approaches ω^2 and can be approximated by eqn (4). Integrating eqn (4) to ω_D yields the Dulong Petit approximation ($3k_B$ per atom) for the heat capacity.

$$C_v = \frac{3\hbar^2}{2\pi^2 k_B T^2}\int_0^{\omega_{max}} \frac{\omega^4 e^{\hbar\omega/k_BT}}{v_g v_p^2 \left(e^{\hbar\omega/k_BT}-1\right)^2} d\omega \quad (3)$$

$$C_{s,HT}(\omega) = \frac{3k_B\omega^2}{2\pi^2 v_g v_p^2} \quad (4)$$

We now consider the frequency dependence of the phonon relaxation time, $\tau(\omega)$.[40] Thermal conductivity is typically limited by a combination of phonon–phonon scattering, point defect scattering and, in nanostructured materials, boundary scattering, which sum according to eqn (5).

$$\tau^{-1} = \sum_i \tau_i^{-1} \quad (5)$$

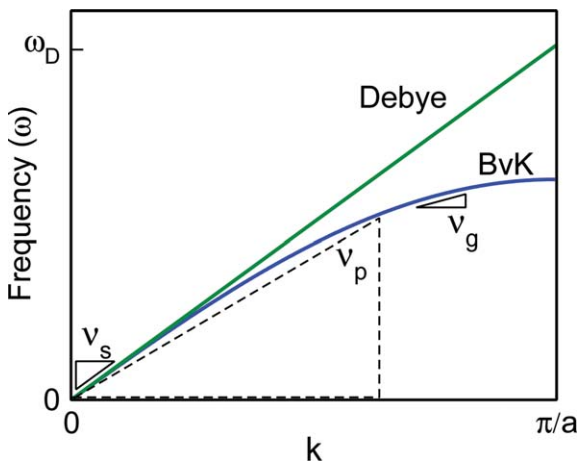

Fig. 2 In a Debye model, the speed of sound (v_s), phase velocity (v_p), and group velocity (v_g) are equivalent. In contrast, a simple Born–von Karman model shows significant curvature of the phonon dispersion.

Variables:

κ_L	lattice thermal conductivity
$\kappa_s(\omega)$	spectral lattice thermal conductivity
C_v	heat capacity
$C_{s,HT}(\omega)$	high temperature spectral heat capacity
$v_g(\omega)$	phonon group velocity, $d\omega/dk$
$v_p(\omega)$	phonon phase velocity, ω/k
v_s	averaged speed of sound
τ	phonon relaxation time
$\bar{M}$	average mass

V	volume per atom
γ	Grüneisen parameter
d	grain or microstructure size
N	atoms per primitive cell
ω	phonon frequency
k	wave vector
a	lattice parameter

At temperatures above θ_D, Umklapp phonon-phonon scattering is often the dominant scattering effect. Umklapp scattering depends strongly on the anharmonicity of the bonding, described by the Grüneisen parameter (γ),[41,42] as well as the average mass ($\bar{M}$), and temperature (T), as seen in eqn (6). Although many expressions exist for τ_U, we emphasize the universality of $\tau_U \propto \frac{\bar{M}v^3}{V^{1/3}\omega^2\gamma^2T}$ and similarity of the pre-factor.[35,43–46] It is instructive to consider the rock salt compounds PbTe and PbSe in the context of eqn (6). While heavier, softer PbTe has a lower group velocity than PbSe, the larger Grüneisen parameter of PbSe leads to similarly low κ_L.[47]

$$\tau_U(\omega) = \frac{(6\pi^2)^{1/3}}{2}\frac{\bar{M}v_g v_p^2}{k_B V^{1/3}\gamma^2\omega^2 T} \quad (6)$$

Boundary scattering in polycrystalline materials with grain size d can be estimated from eqn (7).[48,49] This scattering mechanism is particularly effective in nanostructured materials such as nanowires, thin films, and nanocomposites.[29–31,50]

$$\tau_B = \frac{d}{v_g} \quad (7)$$

Scattering by point defects arises from both mass and strain contrast within the lattice. Point defect scattering has been successfully employed in both thermoelectic materials ($Si_{1-x}Ge_x$), and in thermal barrier coatings, such as yttria stabilized zirconia (YSZ).[1,9] In the simple case of alloying on a single crystallographic site, τ_{PD} is given by eqn (8). Here, f_i is the fraction of atoms with mass m_i and radius r_i that reside on a site with average mass and radius $\bar{m}$ and $\bar{r}$, respectively.[39,51]

$$\tau_{PD}^{-1} = \frac{V\omega^4}{4\pi v_p^2 v_g}\left(\sum_i f_i\left(1-\frac{m_i}{\bar{m}}\right)^2 + \sum_i f_i\left(1-\frac{r_i}{\bar{r}}\right)^2\right) \quad (8)$$

The scattering mechanisms discussed above target different populations of phonons, as shown in Fig. 3(b). Umklapp and point defect scattering target high frequency phonons, while boundary scattering is often the dominant scattering mechanism at low frequencies. In concert, these scattering mechanisms lead to an effective τ shown by the dashed line.

The frequency dependence of the phonon contribution to κ_L can be used to determine which phonons are critical to

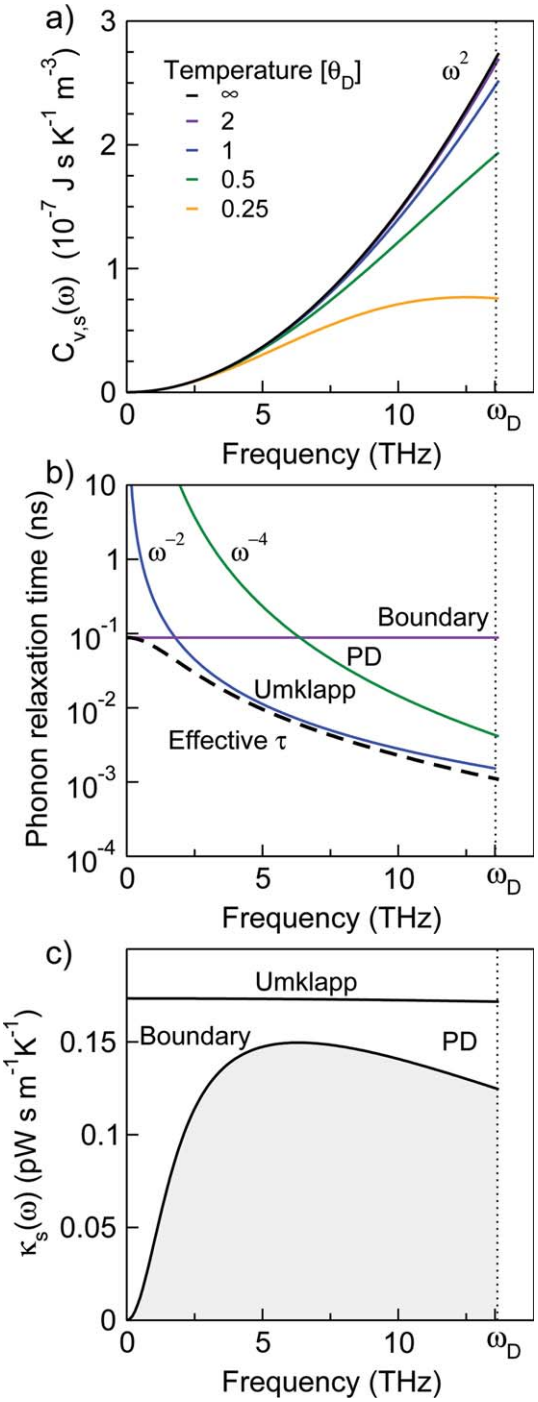

Fig. 3 a) The spectral Debye heat capacity approaches ω^2 dependence at high temperatures. b) Real materials have many scattering mechanisms, which depend heavily on frequency. c) Spectral thermal conductivity (assuming $v_g(\omega) = v_s$ and $T >> \theta_D$) when Umklapp scattering (τ_U) dominates transport (top curve) and when τ_U, τ_B, and τ_{PD} are accounted for (lower curve).

heat transport. The integrand of eqn (2) is commonly referred to as the spectral thermal conductivity, $\kappa_s(\omega) = C_s(\omega)\nu_g(\omega)^2\tau(\omega)$. When thermal conduction is limited by Umklapp scattering, the ω^2 dependence of $C_{s,HT}(\omega)$ is offset by the frequency dependence of Umklapp scattering ($\tau \propto \omega^{-2}$), resulting in the frequency-independent $\kappa_s(\omega)$ curve shown in Fig. 3(c). Integrating over the phonon spectrum yields the classic expression for τ_U-limited κ_L given in eqn (9).[35,45]

$$\kappa_U = \frac{(6\pi^2)^{2/3}}{4\pi^2}\frac{\bar{M}\bar{\nu}_s^3}{TV^{2/3}\gamma^2} \quad (9)$$

This simple expression is commonly invoked to explain high temperature transport, and yields reasonable estimates for κ_L in materials with low mass contrast and simple crystal structures. In most materials, boundary and point defect scattering are also significant, resulting in a highly frequency dependent $\kappa_s(\omega)$. The impact of boundary and point defect scattering on κ_L can be readily visualized as the difference in area between the top and bottom curves of Fig. 3(c).

Thermal conductivity in complex systems

The following sections consider real material systems with phonon dispersions that are progressively more complex than a simple Debye model. Complex phonon dispersions influence κ_L by (a) changing the states available for Umklapp scattering and (b) leading to highly frequency-dependent phonon velocities, as $\nu_g(\omega) = d\omega/dk$.[19,28,52]

Use of a simple Born–von Karman (BvK) model allows us to visualize how chemical structure determines the phonon dispersion. The 1-dimensional BvK model describes the lattice as a chain of atoms connected by springs with harmonic restoring forces.[38,39] Fig. 2 compares the Debye and BvK dispersions for the simple case of a monatomic chain.[53]

High mass contrast. The trend between high mass contrast and low lattice thermal conductivity has been clearly demonstrated by Slack.[28] Fig. 4 reveals that the experimental κ_L of rock salt compounds is dramatically overestimated by the Debye model (κ_U) when mass contrast is high (*e.g.* BaO, mass ratio of 8.6).

The relationship between mass contrast and κ_L can be understood by examining the BvK phonon dispersions for a diatomic chain with varying mass ratio, $m_1 : m_2$ (Fig. 4(b)). When the mass ratio is low, the Debye model's assumption of a constant phonon velocity appears reasonable. However, this assumption breaks down as the mass ratio increases and the optical branch flattens.[54] When τ is limited by Umklapp scattering, the spectral thermal conductivity, $\kappa_s(\omega)$, is proportional to $\nu_g(\omega)^2$. Fig. 4(c) shows the dramatic reduction in $\nu_g(\omega)^2$, and thus κ_L, associated with the flattening of the optical modes with increasing mass contrast. Although not accounted for here, changes to the phonon dispersion may also influence the available states for scattering events, leading to changes in the spectral mean free paths.[55]

High mass contrast likely contributes to the low thermal conductivity found in many of the oxides used for thermal

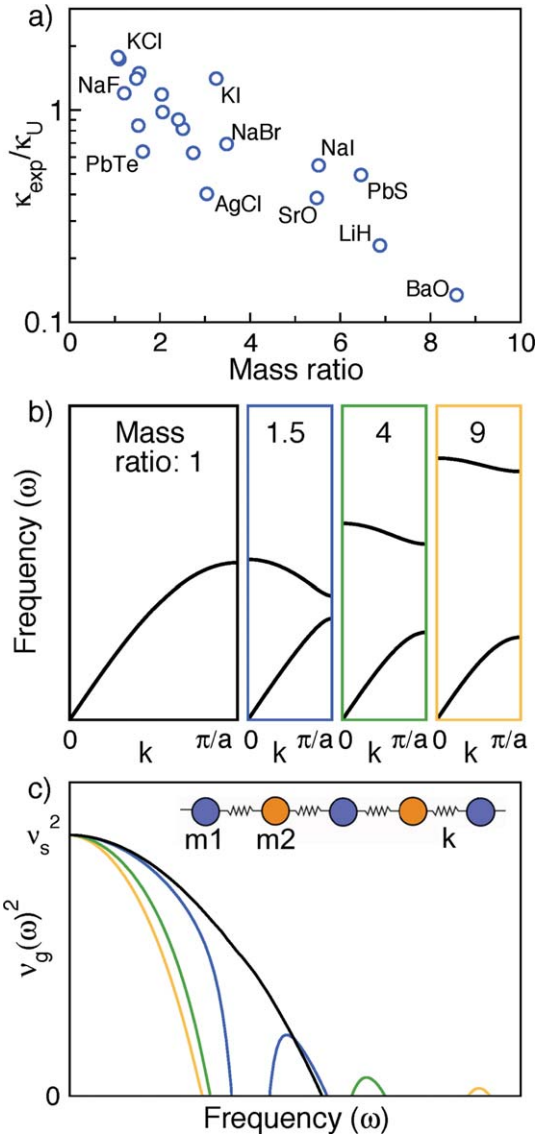

Fig. 4 a) Calculated κ_U significantly overestimates experimental κ_L in rock salt compounds with high mass contrast at $T = \theta_D$. Values for θ_D, γ and κ_L were obtained from Ref. 28. b) This empirical observation can be understood with a BvK model for a 1D diatomic chain. As mass contrast increases (average mass, ν_s held constant) the optical mode flattens and the gap increases. c) When Umklapp scattering dominates, $\kappa_s(\omega) \propto \nu_g(\omega)^2$, and the effect of mass contrast on κ_L can be judged from the area beneath the $\nu_g(\omega)^2$ curves.

Table 1

Material	N	κ_L (300 K) W/mK	Ref.
$LaPO_4$	24	2.5	18
$W_3Nb_{14}O_{44}$	61	1.8	18
$LaMgAl_{11}O_{19}$	64	1.2	56
$La_2Mo_2O_9$	624	0.7	18
α $Al_{14.7}Mn_{3.5}Si_{1.8}$	138	1.5	57
$Ca_5Al_2Sb_6$	26	1.5	58
Ca_3AlSb_3	28	1.6	13
$Yb_{11}Sb_{10}$	42	0.8	59
$Yb_{11}InSb_9$	42	0.8	60
$Ba_8Ga_{16}Ge_{30}$	54	1.1	14,16
$Yb_{14}AlSb_{11}$	104	0.6	15

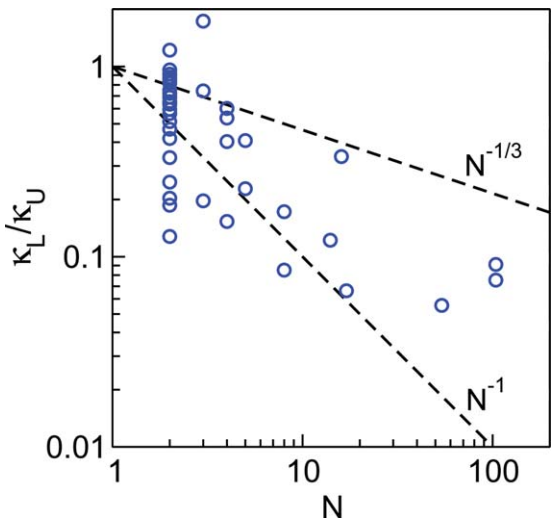

Fig. 5 For materials with many atoms per primitive cell (N), eqn (9) fails to predict the experimental κ_L. See supplemental Table 1.†

barrier coatings (*e. g.*, YSZ has a mass ratio of 5.7). In contrast, most thermoelectric materials have mass contrast less than 2, suggesting a potential avenue for reducing κ_L.

Complex primitive cells. Much like the high mass contrast rock-salt compounds, it has been argued that compounds with a large number of atoms in the primitive unit cell (N) have low κ_L due to low velocity optical modes.[28,43] Classic examples of high-N compounds with low κ_L include $Y_3Al_5O_{12}$ ($N = 80$), β-Boron ($N = 105$), and YB_{68} ($N = 402$).[28,61] More recently, similar trends has been observed in promising materials for thermoelectrics and thermal barrier coatings (Table 1).[12,18]

To further investigate the trend between low κ_L and N, we have compiled the properties of materials for which all of the quantities in eqn (9) are known experimentally. Many materials with applications for thermal barrier coatings have not been included, as their Grüneisen parameters are not reported in the literature. We consider the ratio of measured κ_L to that predicted by κ_U (eqn (9)). Fig. 5 shows that for simple structures, good agreement between κ_U and experimental κ_L is observed. However, the κ_L of more complex materials is grossly over-estimated by the simple κ_U model.

The trend between low κ_L and structural complexity can be qualitatively rationalized by a BvK model. Fig. 6(a) shows phonon dispersions for 1D chains with N-atom cells. As N increases, the phonon dispersion "folds in" on itself, resulting in $N - 1$ optical modes with low $v_g(\omega)$. Thus, in complex materials, the vast majority of heat is trapped in flat, low velocity optical modes, which are not accurately described by a Debye model. Fig. 6(b) emphasizes the reduction of $v_g(\omega)^2$ (and thus $\kappa_s(\omega)$ at the limit of Umklapp scattering), with increasing structural complexity.

For complex materials, a simple approach to modeling κ_L is to consider the acoustic (κ_a) and optical (κ_o) contributions separately. As seen in Fig. 6(a), the acoustic contribution can be treated within a Debye model. To determine the maximum frequency of the acoustic branch, ω_a, we utilize the equal partition of the heat capacity amongst the phonon modes ($C_{v,acoustic} = C_v/N$), yielding $\omega_a = \omega_D/N^{1/3}$.[43] Values for ω_a can thus be obtained either from measurements of v_s or θ_D. However, when inferring ω_a from ω_D, the various approaches to obtaining θ_D (*e. g.*, low or high temperature heat capacity measurements or density of states from neutron experiments) can yield significantly different values.[28,62]

With ω_a determined, κ_a can be determined from eqn (2). For τ limited by Umklapp scattering we find $\kappa_a \propto N^{-1/3}$ (eqn (10)). If instead, boundary scattering is assumed to dominate transport, $\kappa_a \propto N^{-1}$ (eqn (11)). For simplicity, we have used the high temperature limit for the heat capacity. In practice, the experimental N-dependence in Fig. 5(a) is between these bounds, and is consistent with the $N^{-2/3}$ dependence obtained by Slack.[28]

$$\text{Umklapp}: \kappa_a = \frac{(6\pi^2)^{2/3}}{4\pi^2}\frac{\bar{M}v_s^3}{TV^{2/3}\gamma^2}\left(\frac{1}{N^{1/3}}\right) \quad (10)$$

$$\text{Boundary}: \kappa_a = k_B\frac{v_s d}{V}\left(\frac{1}{N}\right) \quad (11)$$

At the amorphous limit ($N = \infty$), the acoustic contribution (κ_a) approaches zero, whereas in practice, glasses still possess finite thermal conductivity. Clearly, we cannot completely ignore the thermal conductivity of the optical modes in which most of the heat in a complex solid is stored. As a lower bound to the optical contribution to thermal conductivity (κ_o), one can look to Einstein's treatment of heat transport as the diffusion of heat between atomic oscillators. Cahill has extended this theory to larger oscillating units, for which $l_{glass} = \lambda/2$, or equivalently $\tau_{glass}(\omega) = \pi/\omega$[63–65] In this model, the speed of sound is used to describe the coupling between oscillators.

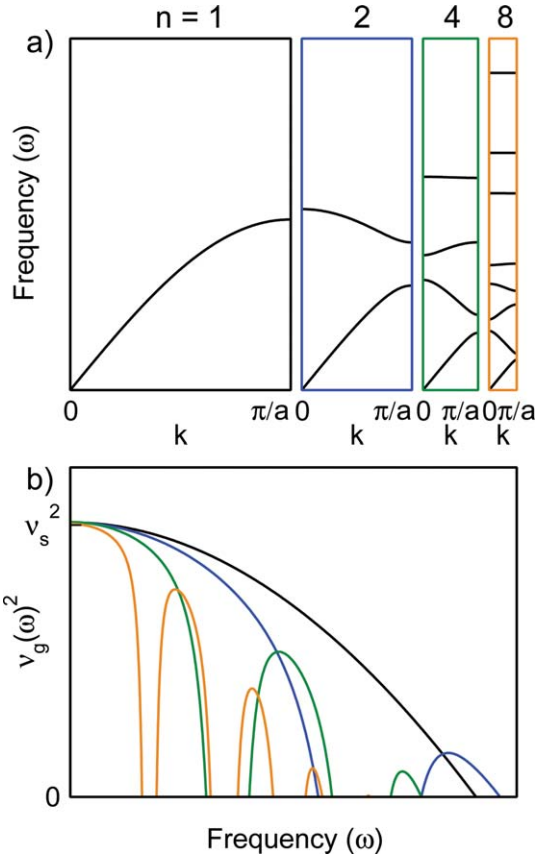

Fig. 6 a) Phonon dispersions for ball and spring chains with increasing number of atoms per unit cell (constant v_s). b) A dramatic decrease in $v_g(\omega)^2$, and thus $\kappa_s(\omega)$, is found with increasing N. For $N = 4$ and 8, the high frequency optical modes are not visible on a linear plot due to the extreme flatness of these modes.

The optical contribution to κ_L, given by eqn (12), is estimated by evaluating eqn (2) with τ_{glass}, a minimum optical frequency of $\omega_D/N^{1/3}$, and the high temperature limit to $C_s(\omega)$. We note that our treatment of optical phonons using a glass model is somewhat unconventional.[66] Optical branches are generally neglected in the modeling of complex materials.

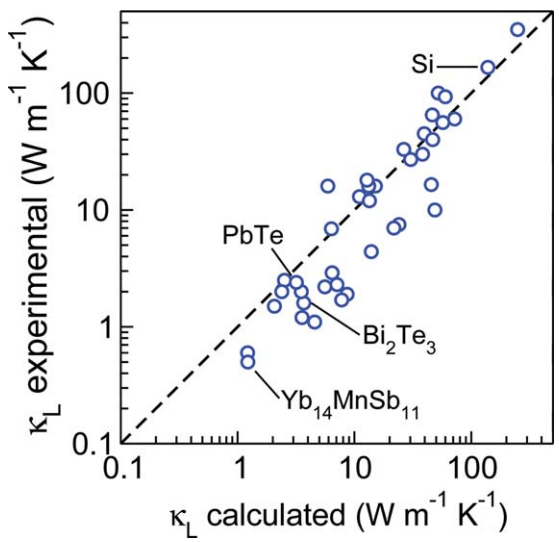

Fig. 7 Success of $\kappa_a + \kappa_o$ in predicting the lattice thermal conductivity of selected materials (see supplementary Table 1†). Here, κ_a includes both Umklapp scattering and a boundary scattering term of 1 μm (eqn (5)).

$$\kappa_o = \frac{3k_B v_s}{2V^{2/3}}\left(\frac{\pi}{6}\right)^{1/3}\left(1 - \frac{1}{N^{2/3}}\right) \qquad (12)$$

Having developed expressions for both the acoustic and optical phonons, we can re-evaluate the thermal conductivity of the materials presented in Fig. 5. We estimate κ_a in a manner analogous to eqn (10) and (11), except that here we assume that both Umklapp and boundary scattering ($d = 1$ μm) limit transport. Summing κ_a and κ_o (eqn (12)) yields good agreement with the experimental κ_L across two orders of magnitude, as illustrated by Fig. 7.

A comparison of $Yb_{14}MnSb_{11}$ and PbTe is particularly revealing. As the bulk properties of these two materials are extremely similar, (θ_D, $\bar{M}$, C_v, γ, see Supplementary Table 1†) κ_U suggests that PbTe should have a slightly lower κ_L than $Yb_{14}MnSb_{11}$. However, calculations accounting for the difference in N predict that the κ_L of $Yb_{14}MnSb_{11}$ ($N = 104$) should be a factor of 3 lower than that of PbTe ($N = 2$) at room temperature. Indeed, the experimental κ_L of $Yb_{14}MnSb_{11}$ and PbTe at 300 K are 0.6 and 2 W m^{-1} K^{-1}, respectively. The success of this incredibly simple approach to modeling extremely complicated thermal transport processes is inspiring. While computational methods may eventually be able to accurately predict thermal conductivity in complex materials, these methods provide valuable intuition.

In the search for low κ_L materials, structural complexity is an elegant approach to achieving glass-like thermal transport across much of the phonon spectrum. Further reduction of thermal conductivity in complex materials can be realized by employing well-established strategies such as: (a) lowering the sound velocity by increasing the density or decreasing the stiffness or (b) including nanostructures to target the remaining acoustic phonons.

Rattling modes. Structural complexity traps heat in glass-like optical modes, but it does not completely eliminate the

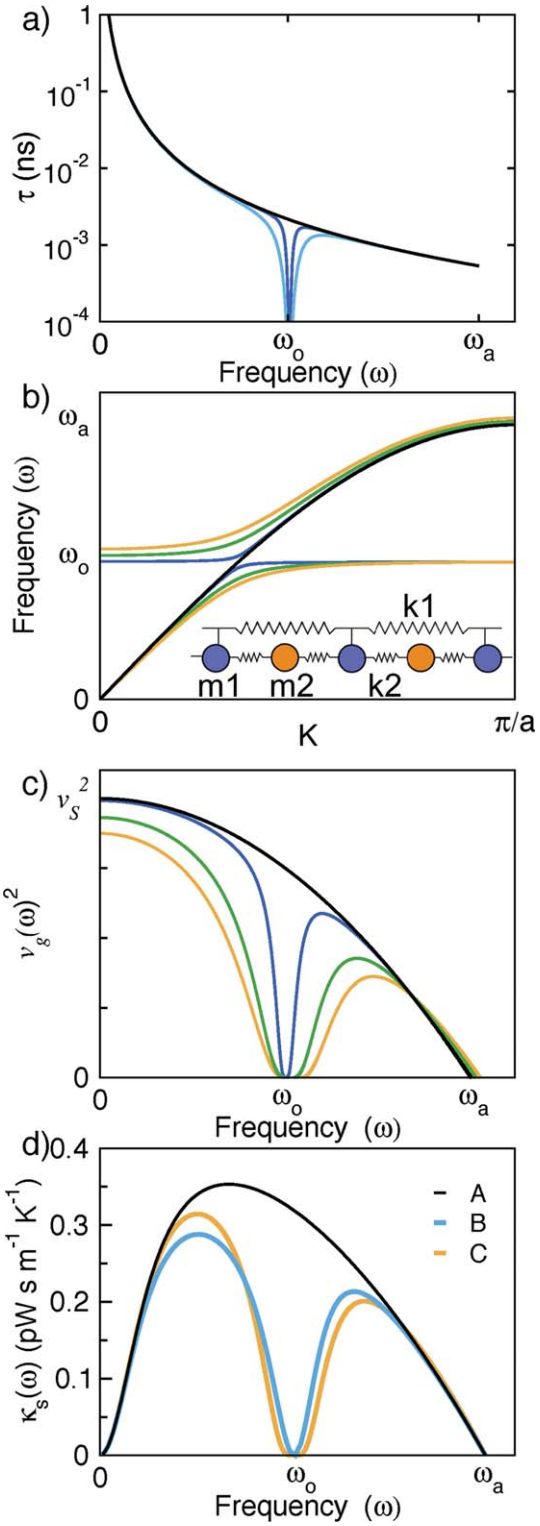

Fig. 8 a) The resonant scattering model targets phonons near ω_o. b) BvK phonon dispersions for a stiff framework (m_1, k_1) and loosely bound guest atoms (m_2, k_2). Increased k_2 stiffness results in increased coupling (extent of avoided crossing) between the framework and guest modes. c) The avoided crossing reduces $\nu_g(\omega)^2$ in the vicinity of ω_o. d) $\kappa_s(\omega)$ for an empty BvK framework, using Umklapp and boundary scattering terms (curve A). Including resonant scattering reduces $\kappa_s(\omega)$ near ω_o (curve B). If instead, the effect of coupling on $\nu_g(\omega)$ is accounted for, a similar reduction is observed (curve C).

contribution from the high-velocity, acoustic branches. One tactic to reduce the acoustic contribution to thermal conductivity has recently arisen in crystal structures with open-frameworks (*e.g.* clathrates and skutterudites).

Guest insertion into open-framework structures can dramatically affect $C_s(\omega)$, $\nu_g(\omega)$, and $\tau(\omega)$. The total heat capacity will increase due to the increased number of atoms per unit volume, potentially increasing κ_L. The phonon relaxation time, τ, may be reduced if the guest atoms have highly anharmonic potentials, leading to increased Umklapp scattering. If the guests only partially occupy the open sites, point defect scattering will also arise.[32] The effect of guest atoms on ν_s will be dictated by the relative change in density and elastic modulus; we would expect that light guest species may actually increase ν_s by stiffening the lattice without dramatically altering the density. In contrast, heavy, weakly bound atoms should lower ν_s.

Much of the excitement surrounding skutterudites and clathrates has been focused on the prediction[66] and observation[67–69] of a phenomena termed "rattling", observed when the guest atom is under-constrained and weakly bound. Experimentally, materials in which guest atoms are strong rattlers are found to exhibit extremely low κ_L.[68,70] While it is widely accepted that rattling atoms result in strongly localized modes within the acoustic frequency range, the mechanism by which rattler modes reduce κ_L is under debate. Historically, the reduction in κ_L has been attributed to resonant scattering by the guest atom.[71] However, the impact of rattling on the group velocity has recently been recognized as an alternative explanation of the low experimental κ_L.[72,73]

Resonant scattering treats the guest atom vibrations as uncorrelated with respect to the framework and other guest species. This scattering mechanism was originally proposed to explain a low temperature indentation in κ_L observed in a solid solution of KCl and KNO_2.[74,75] Fig. 8(a) shows the combined effects of resonant and Umklapp scattering for two different resonant scattering constants. Here, τ is reduced in a narrow frequency range about ω_o, the frequency of the guest atom vibrational mode. This resonant scattering model has successfully been

used to explain the unusual temperature dependence of κ_L for both clathrates and skutterudites.[71,76] However, these models assume a constant group velocity, which fails to capture the complexity of the phonon dispersion and the interaction of the rattling and acoustic modes.

The phonon dispersions of these framework compounds can be investigated using a modified BvK model. We can approximate an empty framework as a monatomic chain of atoms with mass m_1 connected with springs k_1 (black curve, Fig. 8(b)). To simulate the inclusion of guest atoms, we include a second atom with mass m_2 which is coupled to the framework *via* springs (k_2), as shown in Fig. 8(b). At the limit of $k_2 >> k_1$, the lattice behaves as a 2-atom solid with acoustic and optical modes similar to those discussed above in the mass-contrast section.

However, when $k_2 \ll k_1$, the guest species is only loosely bound in the framework and the associated optical mode drops into the same frequency range as the acoustic branch. The interaction of these two modes is manifested as the "avoided crossing" shown in Fig. 8(b) for a range of $k_2 : k_1$ ratios. For this model, we have fixed the framework properties (k_1 and m_1) and the frequency of the rattler mode ($\omega_o \sim \sqrt{k_2/m_2}$). As k_2 stiffens, increased mode mixing is observed. This mixing results in a local reduction of $v_g(\omega)^2$, as illustrated by Fig. 8(c).

The local reduction in group velocity near ω_o has been experimentally observed through inelastic neutron scattering experiments. Measurements of the phonon dispersion of $Ba_8Ga_{16}Ge_{30}$ and $CeRu_4Sb_{12}$ single crystals confirm the presence of rattler modes within the acoustic branch and coupling between these modes.[73,77] In contrast, phonon dispersion measurements of $CeOs_4Sb_{12}$ reveal a conspicuous lack of rattling modes in the acoustic branch. The extremely high framework density, and corresponding low v_s, of $CeOs_4Sb_{12}$ appears to result in acoustic branches that do not reach the guest mode frequency.[78]

Measurements of the heat capacity, phonon density of states and Raman spectra may also be used to observe low frequency guest modes.[67,79–83] The flatness of the guest mode can be deduced from the width of the heat capacity or phonon DOS peak. For example, in the germanium-clathrates, broad peaks observed in the phonon DOS reveal strong coupling between the guest and host modes.[84] Note that while these techniques reveal features in the phonon dispersion, they are insensitive to phonon scattering effects.

Complimenting this experimental work is an increasing body of computational studies which attempt to understand rattling behavior.[81,85–87] The ability to predict the frequency of the rattler mode for different guest species is a particularly attractive feature of this work, helping to guide development of skutterudites with multiple guest elements.[88]

Despite the vast body of research concerning rattling modes, there is an ongoing debate in the community: Is resonant scattering or a local reduction in v_g near the avoided crossing the dominant cause of low κ_L? Fig. 8(d) illustrates the difficulty of distinguishing between these two effects. As a baseline, $\kappa_s(\omega)$ of an empty framework is calculated using τ_U and τ_B and a single-atom, 1-D BvK model for $v_g(\omega)$ (curve A). If resonant scattering is included, a dramatic reduction of $\kappa_s(\omega)$ occurs near ω_o (curve B). However, a similar reduction of $\kappa_s(\omega)$ can be achieved by simply accounting for the reduction in group velocity near ω_o (curve C).[72] Temperature dependent measurements may not be able to distinguish between these effects, as both models in Fig. 8(d) can be used to reproduce the characteristic indentation in κ_L seen in some filled framework materials. It is clear that frequency-dependent measurements of $v_g(\omega)$ and $\tau(\omega)$ will be vital to unravel these intertwined effects on κ_L.

Conclusion

Rational design strategies now exist to guide the discovery and development of advanced thermal materials, heralding a new era for energy materials. Disorder on multiple length scales, from point defects to crystal boundaries, can be used to scatter phonons of different frequencies. Equally influential is the structural complexity of the unit cell, which traps heat in low velocity phonon modes. Resonant phonon modes from "rattling" atoms can be used to reduce the velocity of the remaining acoustic phonons. Despite the intricacies of phonon transport in such complex materials, we find that the thermal behavior can be explained by relatively simple models. These models stress the fundamental *material parameters* which ultimately determine thermal conductivity.

Note added after first publication

This article replaces the version published online on 02 September 2011 and the version published in print, which contained errors where the τ symbols had been incorrectly replaced by σ.

References

1 P. G. Klemens and M. Gell, Thermal conductivity of thermal barrier coatings, *Mater. Sci. Eng.*, 1998, **A245**, 143–149.
2 C. Levi, Emerging materials and processes for thermal barrier systems, *Curr. Opin. Solid State Mater. Sci.*, 2004, **8**, 77–91.
3 D. R. Clarke, Materials selection guidelines for low thermal conductivity in thermal barrier coatings, *Surf. Coat. Technol.*, 2003, **163–164**, 67–74.
4 C. Wood, Materials for thermoelectric energy conversion, *Rep. Prog. Phys.*, 1988, **51**, 459–539.
5 J. R. Sootsman, D. Y. Chung and M. G. Kanatzidis, New and old concepts in thermoelectric materials, *Angew. Chem., Int. Ed.*, 2009, **48**, 8618–8639.
6 G. Chen, M. S. Dresselhaus, G. Dresselhaus, J.-P. Fleurial and T. Caillat, Recent developments in thermoelectric materials, *Int. Mater. Rev.*, 2003, **48**, 45–66.
7 G. J. Snyder and E. S. Toberer, Complex thermoelectric materials, *Nat. Mater.*, 2008, **7**, 105.
8 E. S. Toberer, A. F. May and G. J. Snyder, Zintl chemistry for designing high efficiency thermoelectric materials, *Chem. Mater.*, 2010, **22**, 624–634.
9 C. B. Vining, W. Laskow, J. O. Hanson, R. R. V. der Beck and P. D. Gorsuch, Thermoelectric properties of pressure-sintered $Si_{0.8}Ge_{0.2}$ thermoelectric alloys, *J. Appl. Phys.*, 1991, **69**.
10 P. Yanzhong, A. Lalonde, S. Iwanaga and G. J. Snyder, High thermoelectric figure of merit in heavy-hole dominated PbTe., *Energy Environ. Sci.*, 2011.
11 Y. Z. Pei, *et al.* Synthesis and thermoelectric properties of $KyCo_4Sb_{12}$, *Appl. Phys. Lett.*, 2006, **89**, 221107.
12 C. A. Cox, *et al.* Structure, heat capacity, and high-temperature thermal properties of $Yb_{14}Mn_{1-x}Al_xSb_{11}$, *Chem. Mater.*, 2009, **21**, 1354–1360.
13 A. Zevalkink, E. S. Toberer, W. Zeier, E. Flage-Larsen and G. J. Snyder, Ca_3AlSb_3: an inexpensive, non-toxic thermoelectric material for waste heat recovery, *Energy Environ. Sci.*, 2011, **4**, 510–518.
14 A. F. May, E. S. Toberer, A. Saramat and G. J. Snyder, Characterization and analysis of thermoelectric transport in

n-type $Ba_8Ga_{16-x}Ge_{30-x}$, *Phys. Rev. B: Condens. Matter Mater. Phys.*, 2009, **80**, 125205.
15 E. S. Toberer, *et al.* Traversing the metal-insulator transition in a Zintl phase: rational enhancement of thermoelectric efficiency in $Yb_{14}Al_xMn_{1-x}Sb_{11}$, *Adv. Funct. Mater.*, 2008, **18**, 2795.
16 G. S. Nolas, J. L. Cohn, G. A. Slack and S. B. Schujman, Semiconducting Ge clathrates: Promising candidates for thermoelectric applications, *Appl. Phys. Lett.*, 1998, **73**, 178.
17 C. Uher. & T. M. Tritt, *Skutterudites: Prospective novel thermoelectrics*, 2001, vol. 69, Academic Press, San Diego.
18 M. R. Winter and D. R. Clarke, Oxide materials with low thermal conductivity, *J. Am. Ceram. Soc.*, 2007, **90**, 533540.
19 A. Ward, D. A. Broido, D. A. Stewart and G. Deinzer, Ab initio theory of the lattice thermal conductivity in diamond, *Phys. Rev. B: Condens. Matter Mater. Phys.*, 2009, **80**, 125203.
20 A. Ward and D. A. Broido, Intrinsic phonon relaxation times from first principle studies of the thermal conductivity of Si and Ge, *Phys. Rev. B: Condens. Matter Mater. Phys.*, 2010, **81**, 085205.
21 J. An, A. Subedi and D. J. Singh, Ab initio phonon dispersions for PbTe, *Solid State Commun.*, 2008, **148**, 417–419.
22 J. Dong, O. F. Sankey and C. W. Myles, Theoretical study of the lattice thermal conductivity in Ge framework semiconductors, *Phys. Rev. Lett.*, 2001, **86**, 2361.
23 N. de Koker, Thermal conductivity of MgO periclase from equilibrium first principles molecular dynamics, *Phys. Rev. Lett.*, 2009, **103**, 125902.
24 N. Bernstein, J. L. Feldman and D. J. Singh, Calculations of dynamical properties of skutterudites: Thermal conductivity, thermal expansivity, and atomic mean-square displacement, *Phys. Rev. B: Condens. Matter Mater. Phys.*, 2010, **81**, 134301.
25 R. Berman, *Thermal conduction in solids*, Oxford University Press, Oxford, 1976.
26 *Thermal conductivity: Theory, properties, and applications*, ed. T. M. Tritt, Springer, New York, 2005.
27 D. G. Cahill and R. O. Pohl, Lattice vibrations and heat transport in crystals and glasses, *Annu. Rev. Phys. Chem.*, 1988, **39**, 93–121.
28 G. A. Slack, *Solid State Physics*, 1979, vol. 34, Academic Press, New York.
29 C. J. Vineis, A. Shakouri, A. Majumdar and M. G. Kanatzidis, Nanostructured Thermoelectrics: Big Efficiency Gains from Small Features, *Adv. Mater.*, 2010, **22**, 3970–3980.
30 S. K. Bux, J.-P. Fleurial and R. B. Kaner, Nanostructured materials for thermoelectric applications, *Chem. Commun.*, 2010, **46**, 8311–8324.
31 A. J. Minnich, M. S. Dresselhaus, Z. F. Ren and G. Chen, Bulk nanostructured thermoelectric materials: current research and future prospects, *Energy Environ. Sci.*, 2009, **2**, 466–479.
32 G. P. Meisner, D. T. Morelli, S. Hu, J. Yang and C. Uher, Structure and lattice thermal conductivity of fractionally filled skutterudites: Solid solutions of fully filled and unfilled end members, *Phys. Rev. Lett.*, 1998, **80**, 3551–3554.
33 J. Callaway, Model for lattice thermal conductivity at low temperatures, *Phys. Rev.*, 1959, **113**, 1044–1051.
34 M. G. Holland, Analysis of lattice thermal conductivity, *Phys. Rev.*, 1963, **132**, 2461–2471.
35 P. G. Klemens, Theory of Thermal Conductivity in Solids, in *Thermal Conductivity*, ed. R. P. Tye, 1969, Vol. 1, Academic Press, London.
36 C. Dames and G. Chen, Thermal conductivity of nanostructured thermoelectric materials, in *CRC Handbook of Thermoelectrics*, 2006, CRC Press.
37 D. M. Rowe, V. S. Shukla and N. Savvides, Phonon scattering at grain boundaries in heavily doped fine-grained silicon-germanium alloys, *Nature*, 1981, **290**, 765–766.
38 C. Kittel, *Introduction to Solid State Physics*, 1986, John Wiley and Sons Inc., New York.
39 J. D. Chung, A. J. H. McGaughey and M. Kaviany, Role of phonon dispersion in lattice thermal conductivity modeling, *J. Heat Trans.*, 2004, **126**, 691–696.
40 P. G. Klemens, Thermal conductivity and lattice vibrational modes, *Solid State Phys - Adv. Res. Appl.*, 1972, **7**, 1–98.
41 M. A. Black, Thermal conductivity and anharmonic forces, *Am. J. Phys.*, 1972, **41**, 691–696.
42 J. S. Dugdale and D. K. C. MacDonald, Lattice thermal conductivity, *Phys. Rev.*, 1955, **98**, 1751–1752.
43 M. Roufosse and P. G. Klemens, Thermal-conductivity of complex dielectric crystals, *Phys. Rev. B: Solid State*, 1973, **7**, 5379–5386.
44 G. Leibfried and E. Schloemann, Thermal conductivity of dielectric solids by a variational technique, *Nachr. Akad. Wiss. Goettingen, Math.-Phys. Kl., 2A: Math.-Phys.-Chem. Abt.*, 1954, **23**, 1366–1370.
45 C. L. Julian, Theory of heat conduction in rare-gas crystals, *Phys. Rev.*, 1965, **137**, A128–A137.
46 G. A. Slack and S. Galginaitis, Thermal conductivity and phonon scattering by impurities in CdTe, *Phys. Rev.*, 1964, **133**, A253–A268.
47 H. Wang, Y. Pei, A. D. LaLonde and G. J. Snyder, Heavily doped p-type PbSe with high thermoelectric performance: an alternative of PbTe, *Adv. Mater.*, 2011, **23**, 1366.
48 H. J. Goldsmid and A. W. Penn, Boundary scattering of phonons in solid solutions, *Phys. Lett.*, 1968, **27A**, 523–524.
49 J. E. Parrott, The thermal conductivity of sintered semiconductor alloys, *J. Phys. C: Solid State Phys.*, 1969, **2**, 147–151.
50 S. K. Bux, *et al.* Nanostructured bulk silicon as an effective thermoelectric material, *Adv. Funct. Mater.*, 2009, **19**, 2445–2452.
51 P. G. Klemens, The scattering of low-frequency lattice waves by static imperfections, *Proc. Phys. Soc., London, Sect. A*, 1955, **68**, 1113.
52 M. Blackman, On the heat conduction of simple cubical crystals, *Philos. Mag.*, 1935, **19**, 989.
53 M. Born and T. V. Kármán, *Physik Z.*, 1912, **13**, 297.
54 S. Pettersson, Calculation of the thermal conductivity of alkali halide crystals, *J. Phys. C: Solid State Phys.*, 1987, **20**, 1047–1061.
55 E. F. Steigmeier and I. Kudman, Acoustical-optical phonon scattering in Ge, Si, and iii-v compounds, *Phys. Rev.*, 1966, **141**, 767.
56 C. J. Friedrich, R. Gadow and M. H. Lischka, Lanthanum hexaaluminate thermal barrier coatings, *The 25th An. Int. Conf. on Composites, Advanced Ceramics, Materials, and Structures: B*, 2001, 375–382.
57 T. Takeuchi, N. Nagasako, R. Asahi and U. Mizutani, Extremely small thermal conductivity of the Al-based Mackay-type 1/1-cubic approximants, *Phys. Rev. B: Condens. Matter Mater. Phys.*, 2006, **74**, 054206.
58 E. S. Toberer, A. Zevalkink, N. Crisosto and G. J. Snyder, The Zintl compound $Ca_5Al_2Sb_6$ for low-cost thermoelectric power generation, *Adv. Funct. Mater.*, 2010, **20**, 4375–4380.
59 S. R. Brown, S. M. Kauzlarich, F. Gascoin and G. J. Snyder, High-temperature thermoelectric studies of $A_{11}Sb_{10}$ (A = Yb, Ca), *J. Solid State Chem.*, 2007, **180**, 1414.
60 T. Yi, C. A. Cox, G. J. Snyder and Kauzlarich, High-temperature transport of the Zintl phases $Yb_{11}GaSb_9$ and $Yb_{11}InSb_9$, *Chem. Mater.*, 2010, **22**, 935–941.
61 N. P. Padture and P. G. Klemens, Low thermal conductivity in garnets, *J. Am. Ceram. Soc.*, 1997, **80**, 1018–1020.
62 R. Bruls, H. T. Hintzen and R. Metselaar, On the Debye temperature in the Slack approximation for an estimation of the thermal conductivity of nonmetallic compound, *J. Appl. Phys.*, 2005, **98**, 126101.
63 G. A. Slack. *The thermal conductivity of nonmetallic crystals*, 1979, vol. 34, Academic Press, New York.
64 D. G. Cahill, S. K. Watson and R. O. Pohl, Lower limit to the thermal conductivity of disordered crystals, *Phys. Rev. B: Condens. Matter*, 1992, **46**, 6131–6140.
65 Note that, for most phonon frequencies, $l_{glass} = \lambda/2$ is still much larger than the average distance between atoms. See G. D. Mahan, *Solid State Physics,*1998, Academic Press, New York.
66 G. A. Slack and V. G. Tsoukala, Some properties of semiconducting $IrSb_3$, *J. Appl. Phys.*, 1994, **76**, 1665–1671.
67 V. Keppens, *et al.* Localized vibrational modes in metallic solids, *Nature*, 1998, **395**, 876–878.
68 B. C. Sales, B. C. Chakoumakos, D. Mandrus and J. W. Sharp, Atomic displacement parameters and the lattice thermal conductivity of clathrate-like

thermoelectric compounds, *J. Solid State Chem.*, 1999, **146**, 528–532.
69 M. Christensen, N. Lock, J. Overgaard and B. B. Iversen, Crystal structures of thermoelectric n- and p-type $Ba_8Ga_{16}Ge_{30}$ studied by single crystal, multi-temperature, neutron diffraction, conventional X-ray diffraction and resonsant X-ray diffraction, *J. Am. Chem. Soc.*, 2006, **128**, 15657–15665.
70 P. F. Qiu, *et al.* High-Temperature electrical and thermal transport properties of fully filled skutterudites RFe_4Sb_{12} (R = Ca, Sr, Ba, La, Ce, Pr, Nd, Eu, and Yb), *J. Appl. Phys.*, 2011, **109**, 063713.
71 J. L. Cohn, G. S. Nolas, V. Fessatidis, T. H. Metcalf and G. A. Slack, Glasslike heat conduction in high-mobility crystalline semiconductors, *Phys. Rev. Lett.*, 1999, **82**, 779.
72 M. Zebarjadi, K. Esfarjani, J. Yang, Z. F. Ren and G. Chen, Effect of filler mass and binding on thermal conductivity of fully filled skutterudites, *Phys. Rev. B: Condens. Matter Mater. Phys.*, 2010, **83**, 195207.
73 M. Christensen, *et al.* Avoided crossing of rattler modes in thermoelectric materials, *Nat. Mater.*, 2008, **7**, 811–815.
74 R. O. Pohl, Thermal conductivity and phonon resonant scattering, *Phys. Rev. Lett.*, 1962, **8**, 481–483.
75 M. Wagner, Influence of localized modes on thermal conductivity, *Phys. Rev.*, 1963, **131**, 1443–1455.
76 J. Yang, *et al.* Effect of Sn substituting for Sb on the low temperature transport properties of Ytterbium-filled skutterudites, *Phys. Rev. B: Condens. Matter*, 2003, **67**, 165207.
77 C. H. Lee, I. Hase, H. Sugawara, H. Yoshizawa and H. Sato, Low-lying optical phonon modes in the filled skutterudite $CeRu_4Sb_{12}$, *J. Phys. Soc. Jpn.*, 2006, **75**, 123602.
78 C. P. Yang, *et al.* Phonon dispersion curves in $CeOs_4Sb_{12}$, *J. Phys.: Condens. Matter.*, 2007, **19**, 225214.
79 M. Beekman, R. P. Hermann, A. M. Mochel, F. Juranyi and G. S. Nolas, A study of low-energy guest phonon modes in clathrate-II Na_xSi_{136} (x = 3, 23, and 24), *J. Phys.: Condens. Matter*, 2010, **22**, 355401.
80 M. M. Koza, *et al.* Breakdown of phonon glass paradigm in La- and Ce-filled Fe_4Sb_{12} skutterudites, *Nat. Mater.*, 2008, **7**, 805–810.
81 M. M. Koza, *et al.* Vibrational dynamics of the type-I clathrate $Ba_8Zn_xGe_{46-x-y}\square_y$ (x = 0,2,4,6,8), *Phys. Rev. B: Condens. Matter Mater. Phys.*, 2010, **82**, 214301.
82 Y. Takasu, *et al.* Off-center rattling and cage vibration of the carrier-tuned type-I clathrate $Ba_8Ga_{16}Ge_{30}$ studied by Raman scattering, *Phys. Rev. B: Condens. Matter Mater. Phys.*, 2010, **82**, 134302.
83 G. S. Nolas, *et al.* Raman scattering study of stoichiometric Si and Ge type II clathrates, *J. Appl. Phys.*, 2002, **92**, 7225–7230.
84 R. P. Hermann, *et al.* Neutron and nuclear inelastic scattering study of the Einstein oscillators in Ba-, Sr-, and Eu-filled germanium clathrates, *Phys. Rev. B: Condens. Matter Mater. Phys.*, 2005, **72**, 174301.
85 C. W. Myles, K. Biswas and E. N. Nenghabi, Guest "rattling" impurities in Si and Ge clathrate semiconductors, *Phys. B*, 2007, **401402**, 695–698.
86 E. N. Nenghabi and C. W. Myles, First-principles calculations of the vibrational and thermal properties of the type-I clathrates $Ba_8Ga_{16}Si_xGe_{30-x}$ and $Sr_8Ga_{16}Si_xGe_{30-x}$, *Phys. Rev. B: Condens. Matter Mater. Phys.*, 2008, **78**, 195202.
87 N. P. Blake, S. Latturner, J. D. Bryan, G. D. Stucky and H. Metiu, Band structures and thermoelectric properties of the clathrates $Ba_8Ga_{16}Ge_{30}$, $Sr_8Ga_{16}Ge_{30}$, $Ba_8Ga_{16}Si_{30}$, and $Ba_8In_{16}Sn_{30}$, *J. Chem. Phys.*, 2001, **115**, 8060–8073.
88 J. Yang, W. Zhang, S. Q. Bai, Z. Mei and L. D. Chen, Dual-frequency resonant phonon scattering in $Ba_xR_yCo_4Sb_{12}$ (R = La, Ce, and Sr), *Appl. Phys. Lett.*, 2007, **90**, 192111.

Supplementary Information - Phonon engineering through crystal chemistry

Eric S. Toberer, Alex Zevalkink, G. Jeffrey Snyder
Materials Science, California Institute of Technology, 1200 E. California Blvd. Pasadena, CA 91125,

Compound	Exp. κ_L (W/mK)	N (primitive cell)	$V^{1/3}$ (Å)	θ_D (K)	γ	Calc. κ_L (W/mK)	References
AlSb	56	2	2.83	265	0.6	57	[1, 2]
BaO	2.3	2	2.76	290	1.5	7.1	[2]
BP	350	2	2.27	844	0.75	250	[2]
CdTe	7.5	2	3.24	151	0.52	24	[1, 2]
GaAs	45	2	2.81	277	0.75	39	[2]
GaP	100	2	2.72	346	0.75	52	[2]
GaSb	40	2	3.05	265	0.75	47	[1, 2]
Ge	65	2	2.83	296	0.76	46	[2, 3]
HgTe	2.5	2	3.23	141	1.9	2.5	[4, 5]
InAs	30	2	3.03	208	0.57	38	[2]
InP	93	2	2.92	277	0.6	60	[2]
InSb	16.5	2	3.24	202	0.56	45	[1, 2]
PbS	2.9	2	2.97	230	2	6.4	[2, 3, 6]
PbSe	2	2	3.06	126	1.5	2.4	[2, 7]
PbTe	2	2	3.21	132	1.45	3.5	[2, 8]
Si	166	2	2.70	498	0.56	140	[2, 3]
SnTe	1.5	2	3.15	155	2.1	2.1	[4, 9]
SrO	12	2	2.57	340	1.52	13	[2]
ZnTe	18	2	3.05	195	0.97	13	[2]
ZnS	27	2	2.66	290	0.75	30	[2]
ZnSe	33	2	2.83	239	0.75	26	[2, 3]
Mg_2Ge	13	3	2.79	332	1.38	11	[3]
Mg_2Si	7	3	2.78	476	1.32	22	[3, 10]
Mg_2Sn	16	3	2.95	224	1.27	5.9	[3]
CdS	16	4	2.92	214	0.75	15	[2]
CdSe	4.4	4	3.04	164	0.6	14	[2, 4]
InSe	6.9	4	3.07	190	1.2	6.3	[4]
ZnO	60	4	2.29	481	0.75	72	[2]
Bi_2Te_3	1.6	5	3.24	155	1.49	3.7	[4, 11]
Sb_2Te_3	2.4	5	3.15	160	1.49	3.2	[4]
$CuGaTe_2$	2.2	8	3.00	226	1.46	5.6	[4, 12]
InTe	1.7	8	3.17	186	1	7.8	[4, 13]
La_2Te_3	1.2	14	3.17	208	1.76	3.6	[14]
$CoSb_3$	10	16	2.85	307	0.95	49	[15]
$IrSb_3$	16	16	2.91	308	1.42	13	[16]
$CeFe_4Sb_{12}$	1.9	17	2.82	287	1.42	8.7	[17]
$Ba_8Ga_{16}Ge_{30}$	1.1	54	2.86	300	1.6	4.6	[18, 19]
$Yb_{14}AlSb_{11}$	0.6	104	3.07	160	1.5	1.2	[20]
$Yb_{14}MnSb_{11}$	0.5	104	3.07	160	1.5	1.2	[20]

TABLE I: Summary of the data which was used to calculate Figure 5 and 7 in the text. Our survey of the literature suggests fairly few compounds are sufficiently characterized for calculation of κ_L. Here, the calculated κ_L is the sum of κ_a and κ_o. The κ_a is obtained by solving Eq. 2 for a combination of Umklapp and boundary scattering (d =1 μm) limit with $\omega_m ax = \omega_a$ and $C_s(\omega) = C_{s,HT}(\omega)$. The κ_o is determined from Eq. 12.

[1] Garbato, L. & Rucci, A. Ionicity dependence of lattice thermal conductivity in tetrahedral semiconductors. *Chem. Phys. Lett.* **61**, 542 – 544 (1979).
[2] Morelli, D. T. & Slack, G. A. *High Thermal Conductivity Materials*, chap. High lattice thermal conductivity solids, 37–64 (Springer: New York, NY, 2005).
[3] Slack, G. A. *Solid State Physics*, vol. 34 (Academic Press, New York, 1979).
[4] Spitzer, D. P. Lattice thermal conductivity of semiconductors: A chemical bond approach. *J. Phys. Chem. Solids* **31**, 19 (1970).
[5] Khattak, G. D., Akbarzadeh, H. & Keesom, P. H. Specific heats of mercury chalcogenides and HgI_2 between 0.4 and 50 K. *Phys. Rev. B* **23**, 2911–2915 (1981).
[6] Parkinson, D. H. & Quarrington, J. E. The molar heats of lead sulphide, selenide and telluride in the temperature range 20 K to 260 K. *Proc. Phys. Soc.* **67**, 569 (1954).
[7] Wang, H., Pei, Y., LaLonde, A. D. & Snyder, G. J. Heavily doped p-type PbSe with high thermoelectric performance: an alternative for PbTe. *Adv. Mat.* (2011).
[8] Yanzhong, P., Lalonde, A., Iwanaga, S. & Snyder, G. J. High thermoelectric figure of merit in heavy-hole dominated pbte. *Energy and Env. Science* (2011).
[9] Smith, T. F., Birch, J. A. & Collins, J. G. Low-temperature heat capacity, thermal expansion and Grüneisen parameters for SnTe. *J. Phys. C: Solid State Phys.* **9**, 4375 (1976).
[10] Bux, S. K. *et al.* Mechanochemical synthesis and thermoelectric properties of high quality magnesium silicide, submitted (2011).
[11] Shoemake, G. E., Rayne, J. A. & Ure, R. W. Specific Heat of *n*- and *p*-Type Bi_2Te_3 from 1.4 to 90K. *Phys. Rev.* **185**, 1046–1056 (1969).
[12] Thermal conductivity of $CuGaTe_2$. *Solid State Comm.* **64**, 439 – 442 (1987).
[13] Alicy, N. C., Kerimov, I. C. & Kurbanov, M. M. *Sov. Phys. Solid State* **14**, 3106 (1973).
[14] May, A. F., Fleurial, J.-P. & Snyder, G. J. Thermoelectric performance of lanthanum telluride produced via mechanical alloying. *Phys. Rev. B* **78**, 125205 (2008).
[15] Morelli, D. *et al.* Low-temperature transport-properties of p-type $CoSb_3$. *Phys. Rev. B* **51**, 9622–9628 (1995).
[16] Slack, G. A. & Tsoukala, V. G. Some properties of semiconducting $IrSb_3$. *J. Appl. Phys.* **76**, 1665–1671 (1994).
[17] Morelli, D. T. & Meisner, G. P. Low temperature properties of the filled skutterudite cefe4sb12. *J. Appl. Phys.* **77**, 3777–3781 (1995).
[18] Sales, B. C., Chakoumakos, B. C., Jin, R., Thompson, J. R. & Mandrus, D. Structural, magnetic, thermal, and transport properties of $X_8Ga_{16}Ge_{30}$ (X=Eu, Sr, Ba) single crystals. *Phys. Rev. B* **63**, 245113 (2001).
[19] May, A. F., Toberer, E. S., Saramat, A. & Snyder, G. J. Characterization and analysis of thermoelectric transport in n-type $Ba_8Ga_{16-x}Ge_{30-x}$. *Phys. Rev. B* **80**, 125205 (2009).
[20] Cox, C. A. *et al.* Structure, Heat Capacity, and High-Temperature Thermal Properties of $Yb_{14}Mn_{1-x}Al_xSb_{11}$. *Chem. Mater.* **21**, 1354–1360 (2009).